Effect of crowning radius on rolling contact fatigue strength for traction drive elements

Effect of crowning radius on rolling contact fatigue strength for traction drive elements (Evaluation by simulation)

Yukihito NARITA*, Naoto KATO**, Masashi YAMANAKA***, Toshiharu KAZAMA*, Yasuhiro OSAFUNE* and Tomoya MASUYAMA****

*Muroran Institute of Technology,
27-1 Mizumoto-cho, Muroran 050-8585, Japan
E-mail: y-narita@mmm.muroran-it.ac.jp
**Division of Mechanical Systems and Materials Engineering, Muroran Institute of Technology,
27-1 Mizumoto-cho, Muroran 050-8585, Japan
***High Energy Accelerator Research Organization,
1-1 Oho, Tsukuba, Ibaraki 305-0801, Japan
****Tsuruoka National College of Technology,
104 Inooka-sawada, Tsuruoka, Yamagata 997-8511, Japan

Received 20 June 2014

Abstract

A simulation of the rolling contact fatigue strength of a traction drive element was developed. This simulation accounts for both the distribution of sizes of inclusions in the element material and the influence of traction forces at the element surface. The shear strength of the matrix structure surrounding an inclusion was estimated with an equation. The hardness distribution and the Weibull distribution of inclusion dimensions, which are necessary parameters to calculate the rolling contact fatigue strength, were determined by observation of an actual test specimen. The purpose of this report is simulations to evaluate the effect of the crowning radius on the rolling contact fatigue strength and the torque capacity. The simulations were carried out by varying the crowning radius of the virtual roller. To consider the effect of the crowning radius, a simulated two-dimensional virtual roller, which has actual material properties, was modified to a roller multilayered toward the axial direction. The simulation assuming the actual roller led to a difference of 1.0% from the experimental rolling contact fatigue strength. This difference was 2.4 points smaller than the result for the two-dimensional virtual roller. The rolling contact fatigue strength decreased with increasing crowning radius for two reasons. One was the increase in the number of inclusions under the high stress due to the increasing crowning radius. The other was the expansion of the portion of the roller subject to high stresses down to a depth having small hardness. However, the torque capacity calculated from the contact force resulting in failure increased with the increasing crowning radius.

Key words : Machine element, Traction drive, Rolling contact fatigue, Inclusion, Tribology, Shear stress

1. Introduction

A traction drive transmits power through shear forces in the elastohydrodynamic lubrication film between pairs of rollers. Traction drives have several advantages over gears, notably, lower vibration and noise, and usefulness in the assembly of continuously variable transmissions (CVT). Since contact forces play an integral role in traction drives for power transmissions, high contact pressures occur at the points of contact between rollers. For example, toroidal CVTs for automobiles are operated at maximum Hertzian pressures exceeding 4 GPa (Machida et al., 1995). These high contact pressures cause failure through rolling contact fatigue, which occurs in bearings and gears. The most common mode of failure is surface flaking. Therefore, prediction of the rolling contact fatigue strength is essential during the design of a traction drive.

A number of studies have reported the fatigue strength in traction drives. Many kinds of fatigue tests have been

carried out on rollers and balls to examine the influence of failure mechanisms, operating conditions, lubrication modes, roller materials, etc., on fatigue strength (Machida et al., 1993; Deng et al., 1999; Nakajima and Mawatari, 2005; Matsuo et al., 1991; Coy et al., 1981; Rohn et al., 1981). Murakami (2002) proposed an equation for predicting the fatigue limit, which considers the size of microdefects or inclusions. Yamanaka et al. (2012) proposed a prediction equation for estimating the rolling contact fatigue strength of traction drive elements by extending Murakami's method.

It is well known that the high-strength materials employed in traction drives and gears show high scatter in fatigue strength (Murakami et al., 1988). A large number of fatigue tests must be performed to estimate the scatter. It would be very useful for strength design if the scatter could be estimated by simulation. The authors developed a simulation analysis of the rolling contact fatigue strength of traction drive elements (Narita et al., 2013) by accounting for both the distribution of sizes of inclusions in the element material and the influence of traction forces employing Masuyama's method (Masuyama et al., 2002a). When a simulation was performed using the same material with the same distribution of inclusions measured in the test rollers and assuming the traction coefficient found in the experiment, the calculated rolling contact fatigue strength matched the experimental findings with an error of 2.5%.

For a traction drive to transmit high torques, the contact force must be raised in proportion to the desired increase in torque. It is common to increase the crowning radius of the roller to avoid raising the contact pressure at the same time. The crowning radius is thought to affect the rolling contact fatigue strength of traction drives. Yoshida et al. (1998) conducted a rolling contact fatigue test on case-hardened rollers of Japan Industrial Standard (JIS) SCM415H chromium molybdenum steel with three different crowning radii and lubricated with gear oil, and reported that lifetime and surface durability diminished with increasing crowning radius. The experimental conditions were a slip ratio of 20% and roller surface roughness R_a of several μm; both of these were set an order of magnitude or more higher than the actual values in a typical traction drive. Therefore, the failure mode in these rollers was cracks on the surface and wear. Their research results should not be applied as-is to traction drives. Yoshida et al. (1989) also conducted rolling contact fatigue tests in carbonitrided rollers of JIS SCr420 chromium steel with varying diameters and case depths. The failure mode there was spalling caused by subsurface cracking in the roller. Uncrowned (flat) rollers were used in the test, so line contact occurred between the rollers. Traction drives are mainly employed in CVTs, so, in most cases, the contact patch of the roller is elliptical with attendant high contact pressures. For this reason, the results of this report are also difficult to apply to traction drives. Fujii et al. (2007) carried out rolling fatigue tests on quenched rollers of JIS SUJ2 high carbon chromium bearing steel lubricated with turbine oil to examine the influence of the shape of the contact patch on the rolling contact fatigue and on the failure mode. Their tests were carried out with rollers combining convex, flat and concave crowning, and the slip ratio was high at approximately 20%. Because of this, the failure mode of rollers having an elliptical contact patch was pitting originated at surface cracking sites. Thus, no known studies have examined the influence of the roller crowning radius and the mechanisms on rolling contact fatigue failure of traction drives, in which the failure mode generally initiates at an internal site.

In this study, a previously developed simulation of the rolling contact fatigue strength of the elements of a traction drive was improved to allow consideration of the crowning radius. Simulations were then conducted with various crowning radii, and the influence of the crowning radius on the rolling contact fatigue strength of a traction drive and the torque capacity were observed.

2. Criterion of rolling contact fatigue

During rolling contact fatigue, cracks propagate parallel to the rolling direction. Therefore, as in previous research, we again concentrated on the shear stress parallel to the rolling direction, τ_{zx}. These cracks initiate from the inclusions and defects within the material and propagate to the point of failure by this τ_{zx}. This study uses the following criteria for the failure from a given defect in a traction drive element: rolling contact fatigue strength τ_w is assumed around a defect, and failure is assumed to occur if the shear stress τ_{zx} due to the contact force F_c, which is normal to the contact point, exceeds τ_w. The prediction equation for τ_w, defined as the rolling contact fatigue strength for 10^7 cycles, is given below (Yamanaka et al., 2012):

$$\tau_w = c \times \frac{1.56(Hv + 120)}{\left(\sqrt{area}\right)^{1/6}} \tag{1}$$

where *Hv* is Vickers hardness and *area* is the projected area of an inclusion onto a plane perpendicular to the evaluation stress. Coefficient *c* is assigned the value 0.97 on the basis of the rolling contact fatigue strength found in a preliminary experiment using rollers with artificially induced defects of determined dimensions.

3. Simulation of rolling contact fatigue strength considering crowning radius

3.1 Problem of previous simulation

The model for the calculations in a previous simulation (Narita et al., 2013) was a two-dimensional virtual roller that intersected the center of the Hertzian contact patch of the roller. "Virtual roller" means a computer model of a roller containing the same distribution of inclusions and surface hardness as an actual roller. We examined how the shear stress τ_{zx} varies with respect to the roller rotational axial direction, as shown in Fig. 1. The results show that τ_{zx} is high even at locations distant from the center ($y = 0$) of the Hertzian contact ellipse. Therefore, it is conceivable that failure occurs at locations distant from the center of the Hertzian contact ellipse. Also, if the crowning radius is modified to obtain a constant roller rotation radius and a constant Hertzian pressure, the radius of the Hertzian contact ellipse changes slightly in the rolling direction of the roller (see Fig. 2), but the radius changes very much in the axial direction of the roller. Also, as indicated in Fig. 1, the variation in τ_{zx} is affected by the crowning radius r_c. Consequently, the previous simulations cannot accurately predict the influences of the crowning radius r_c.

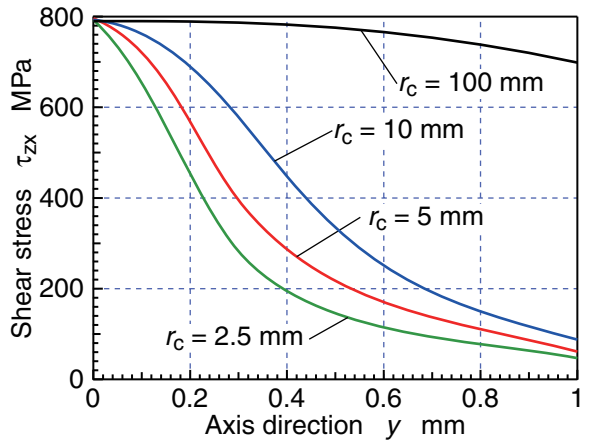

Fig. 1 Changing shear stress with distance from contact center toward axis direction

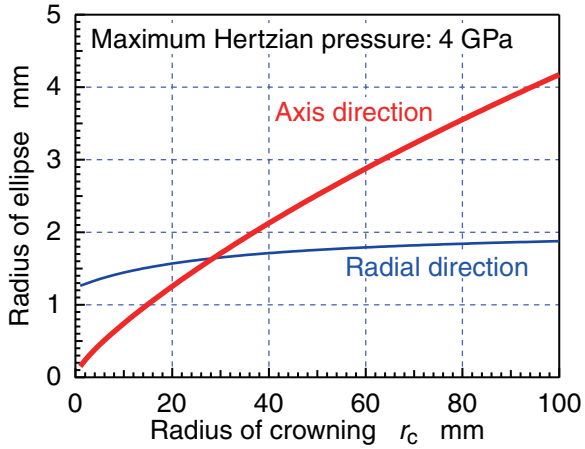

Fig. 2 Changing radius of contact patch with crowning radius

3.2 Multilayered virtual roller

The method of simulation was improved with the objective of solving the above issues. Masuyama et al. (2002b) assumed an isotropic distribution of inclusions when evaluating the bending fatigue strength of a tooth root of a carburized gear in a simulation, and approximated the distribution of inclusions in the tooth width direction by combining two-dimensional virtual gear models in layers. The same method was used in this study. Specifically, a simplified three-dimensional virtual roller model was created by combining the previous two-dimensional virtual roller models with simulations of layers in the axial direction (Fig. 3). It was vital to determine the spacing between each layer so that the model would be equal to the inclusion density of the actual material. Masuyama et al. set the layer spacing at the mean distance between inclusions, and that value was used in this study as well.

Figure 4 is a histogram of the inclusion sizes determined by the observation of a specimen (Narita et al., 2013). A test specimen was made of pre-quenched SCM415H. The bar stock used to build the rollers was cut with a fine cutter and buffed to create the specimen. The number of inclusions and the surface area of each inclusion on the surface of the specimen were measured under a digital microscope (Keyence VH-8000, 2.11 megapixels). A total of 200 mm^2 of surface was examined. According to the research on SUJ2 by Hiroshi Murakami, inclusions less than $\sqrt{area}$ = 2 μm do not affect the fatigue life of a roller (Murakami, 2000); that is, such inclusions do not become the initiation sites of failure. In view of that report and the limits of precision of the digital microscope, we decided not to measure inclusions less than the size of 1 μm^2. It should be noted that the greater the inclusion size, the lower the frequency of occurrence. The inclusion density was 107/mm^2. The mean distance between inclusions calculated from this density is

0.097 mm. On this basis, the layer spacing in the virtual roller was set at 0.1 mm.

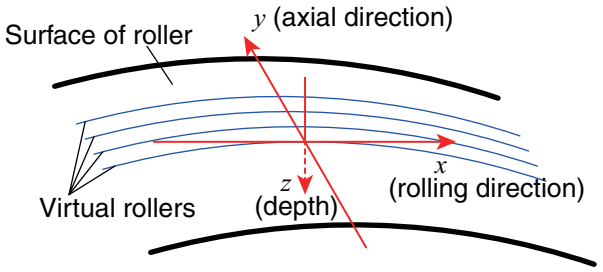

Fig. 3 Schematic and coordinates of virtual multilayered roller

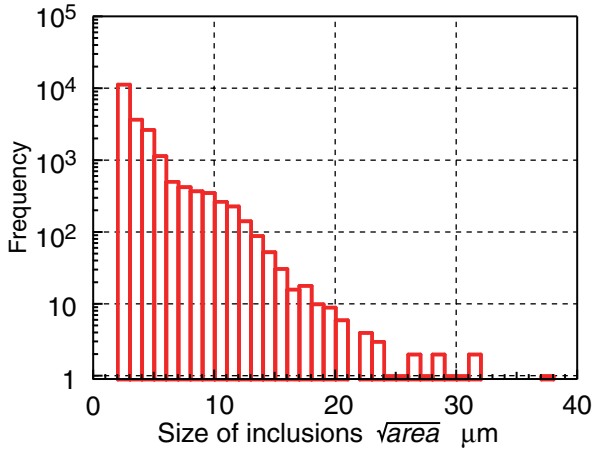

Fig. 4 Histogram of size of observed inclusions

3.3 Procedure of improved simulation

Figure 5 is a flow chart of the improved version of the simulation. First, inclusions were distributed in each layer of the virtual roller. The distribution of inclusion dimensions followed a composite Weibull distribution, as determined in observations of a specimen of the roller material SCM415H (Narita et al., 2013). The following equations provide the composite Weibull distribution:

$$Y_1 = \ln\left(\ln\frac{1}{1-F(t)}\right) = m_1 \ln t - m_1 \ln \eta_1 \qquad (0 < F(t) < \delta) \tag{2}$$

$$Y_2 = \ln\left(\ln\frac{1}{1-F(t)}\right) = m_2 \ln t - m_2 \ln \eta_2 \qquad (\delta < F(t) < 1) \tag{3}$$

where $F(t)$ is the cumulative distribution percentage, m is the shape parameter, η is the scale parameter, and δ is the separation parameter. In this study, the Weibull random number was $t = \sqrt{area}$. As can be seen from the equations, the plot of Y with respect to $\ln t$ is a linear function. We can obtain m and η from the slope of the line and the intercept, respectively. The separation parameter δ in Eqs. (2) and (3) can be found by using intersection t_c of the two above lines:

$$t_c = \frac{m_1 \ln \eta_1 - m_2 \ln \eta_2}{m_1 - m_2} \tag{4}$$

Figure 6 combines the Weibull plot of the measured inclusion area $\sqrt{area}$ shown in Fig. 4 and the linear approximations of these results obtained from Eqs. (2) and (3). Table 1 provides the Weibull parameters obtained from

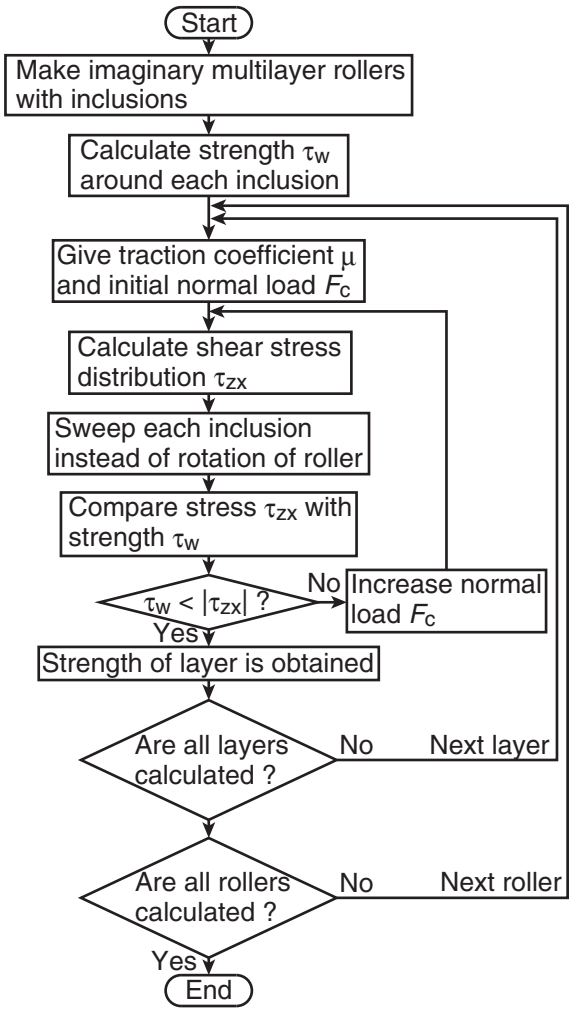

Fig. 5 Flow chart of simulation

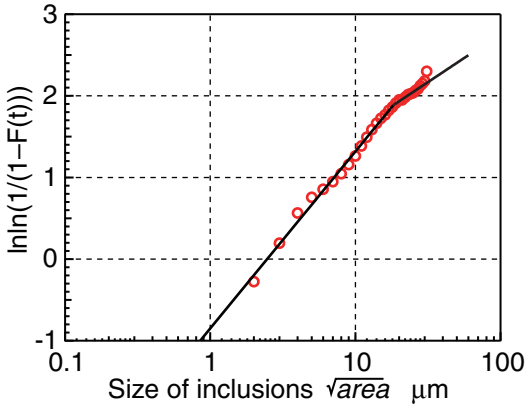

Fig. 6 Weibull plot of distribution of inclusions

Table 1 Weibull parameters

Weibull parameter m_1	0.942
Weibull parameter m_2	0.514
Weibull parameter η_1	2.467
Weibull parameter η_2	0.467
Boundary t_c	18.28

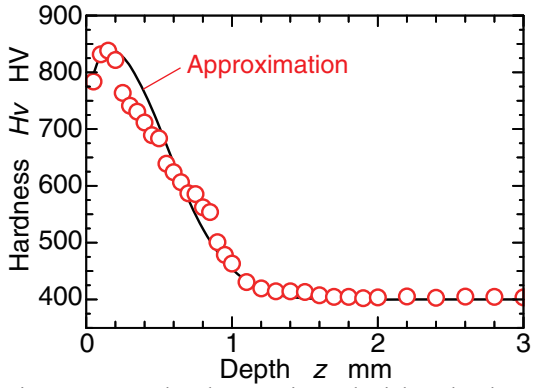

Fig. 7 Measured and approximated Vickers hardness (Narita et al., 2013)

the linear approximations. To obtain the reciprocal functions of Eqs. (2) and (3), we find:

$$t = \eta\left[-\ln\left(1-F(t)\right)\right]^{\frac{1}{m}} \tag{5}$$

Uniform random numbers were applied in $F(t)$ over the semi-open interval [0,1) to numerically obtain the Weibull random number $t = \sqrt{area}$. These random numbers were used to randomize the locations of the inclusions. This process allowed us to create virtual rollers that have the distribution of inclusion dimensions and density found in the actual material. Inclusions were placed in each layer of the virtual roller by the same method, and their locations were recorded in terms of depth z beneath the roller surface and angular location θ in the circumferential direction. It must be noted that in a few rare cases, huge inclusions were generated. These inclusions lowered the fatigue strength. In such cases, the maximum value $\sqrt{area}_{\max}$ = 69 μm for the inclusion area was estimated with the statistics of extremes (Murakami, 2002) and used as the upper limit of the $\sqrt{area}$ of generated inclusions (Narita et al., 2013).

Using Eq. (1), we next calculated the rolling contact fatigue strength in the vicinity of an inclusion. For hardness Hv, required in this equation, we applied the values observed in experiments with actual rollers (Yamanaka et al., 2012; Narita et al., 2013). The material was carburized SCM415H. Figure 7 presents the measured hardness in the depth direction. The maximum hardness was 840 Hv, and it occurred at a depth of 0.2 mm below the roller surface. The

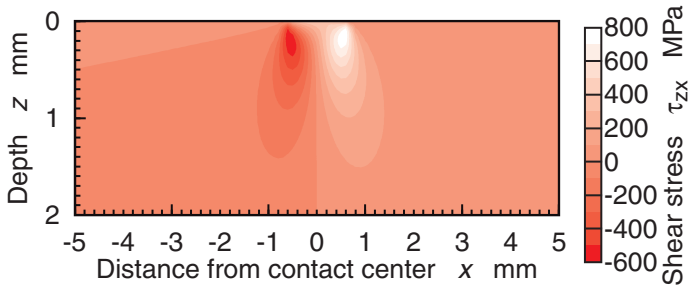

Fig. 8 Shear stress τ_{zx} of driven roller (F_c = 1800 N)

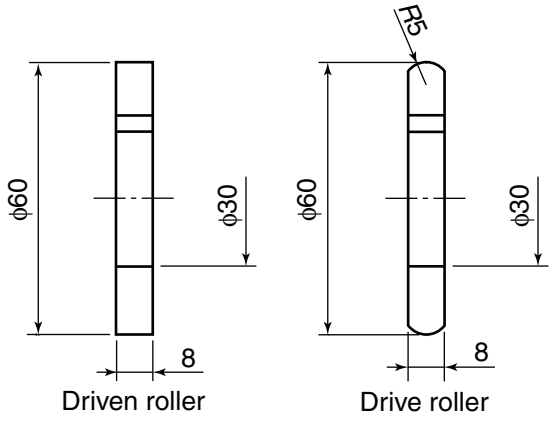

Fig. 9 Shape and dimensions of test roller pair

surface hardness was 750 *Hv*, the core hardness was 400 *Hv*, and the effective case depth was 0.8 mm. We applied the approximated values obtained from experiments with actual rollers as shown in Fig.7 (Narita et al., 2013).

Next, the shear stresses τ_{zx} occurring in each layer of the virtual roller were calculated by using the commercial boundary element method program TED/CPA (TriboLogics Corporation) (Kakoi 1991). This program can calculate the internal stresses in the roller occurring from frictional forces at the surface. Here, the friction coefficient, $\mu = 0.12$, was set equal to the traction coefficient found in an experiment (Yamanaka et al., 2012). Young's modulus of the roller material SCH415H is 207.5 GPa and Poisson's ratio is 0.3. Particularly high stresses occur in the vicinity of the contact point in Hertzian contact. To reduce the execution time, calculations were only carried out for the inclusions distributed in the virtual roller within a depth of $z \leq 2$ mm below the roller surface. The calculation region for the stress distribution was placed with its origin at the contact point in the area $0 \leq z \leq 2$ mm in the depth direction and $-5 \leq x \leq 5$ mm in the rolling direction. Rolling was in the positive x direction. The increments in the x and z directions were 0.025 mm and 0.005 mm, respectively. The coordinate system is shown in Fig. 3. Figure 8 provides an example of the distribution of τ_{zx} at $y = 0$ under the contact force F_c = 1800 N. The roller was the same shape as those used previously, as shown in Fig. 9 (Yamanaka et al., 2012; Narita et al., 2013). The vertical scale in Fig. 8 is double that of the horizontal scale. This figure shows that τ_{zx} increases in the $x > 0$ region under traction force. Here, as shown in Fig. 1, the shear stress τ_{zx} also varies in the y direction, the roller axial direction. Consequently, we must also determine the calculation range in the y direction as appropriate to the roller crowning radius. The calculation range is addressed below.

Finally, instead of rotating the roller, each inclusion was shifted toward the rolling direction in the stress distribution and the rolling contact fatigue strength τ_w, calculated in Eq. (1), was compared with τ_{zx}. Since the sign of τ_{zx} changes about the roller contact point, $|\tau_{zx}|$ was compared. Failure was assumed to occur when $\tau_w < |\tau_{zx}|$, and the fatigue strength for that case was recorded. When failure occurred from multiple inclusions, the inclusion with the lowest τ_w was designated as the failure initiation site. When no failure occurred, the contact force F_c was increased, the stress distribution was re-calculated, and the comparison of the fatigue strength with $|\tau_{zx}|$ was repeated. Once failure occurred, it was transmitted to the neighboring layers, and the above procedure was repeated for all layers. The layer with the lowest F_c at the time of failure was then designated the failure initiation site in the virtual roller. This process was repeated for a given number of simulated rollers, and histograms of the fatigue strength were output.

3.4 Effect of multilayered virtual roller

We carried out a simulation of the rolling contact fatigue strength of rollers observed in previous rolling fatigue tests (Yamanaka et al., 2012; Narita et al., 2013) and validated the effectiveness of changing over to the multilayered model. As shown in Fig. 9, the test rollers were cylindrical with a diameter of 60 mm. The driving roller had a crowning radius r_c of 5 mm and the driven roller was flat. The driven roller was the object of the simulation here. The range of layers of the virtual roller was set such that the maximum τ_{zx} ($\tau_{zx\ max}$) in a layer, which should be the most separated layer from the center (y = 0 mm) of the Hertzian contact ellipse, decreased from 50% of $\tau_{zx\ max}$ of the layer passing through y = 0 mm. TED/CPA (Kakoi 1991) predicted the range y = −0.4 to +0.4 mm. As described in the previous section, the increment of y was 0.1 mm; thus, a single virtual roller consisted of 9 layers. For this simulation, 1000 different virtual rollers were created, and this was 10 times the greatest number previously created (Narita et al., 2013). The calculations were carried out while increasing the contact force F_c in steps of 50 N. For comparison, calculations were also performed for a single-layer roller model (Narita et al., 2013). To ensure a fair comparison, the layer on the y = 0 mm plane in the multilayered roller had an inclusion distribution identical to that in the single-layer roller.

Figure 10 is a histogram of the rolling contact fatigue strength obtained in the simulations. The colored bars indicate the simulations in the previous single-layer rollers; the white bars indicate the present multilayered rollers. Figure 11 provides a plot of these results on normal probability paper. The points representing each of the two models fall into straight lines, indicating that the simulation results generally followed a normal distribution. These figures were used to calculate the rolling contact fatigue strength resulting in a failure probability of 50%. The fatigue strength was 817 MPa for the single-layer roller and 798 MPa for the multilayered roller. The standard deviations of these values were nearly identical: 41.5 MPa for the single-layer roller and 39.9 MPa for the multilayered roller. As seen in Fig. 10, creating a multilayered model for the virtual roller results in decreased mean strength despite nearly identical scatter of predicted strength.

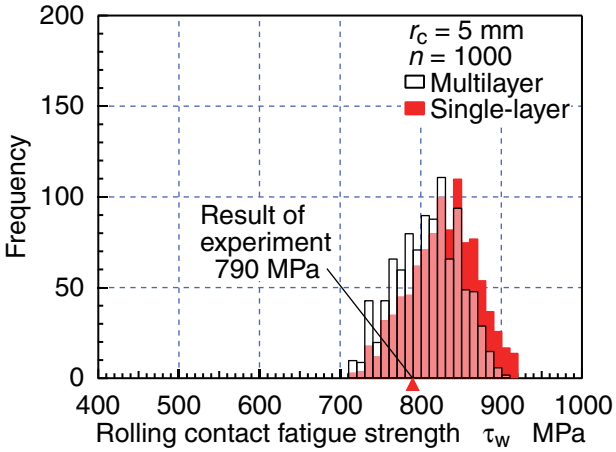

Fig. 10 Rolling contact fatigue strength (r_c = 5 mm)

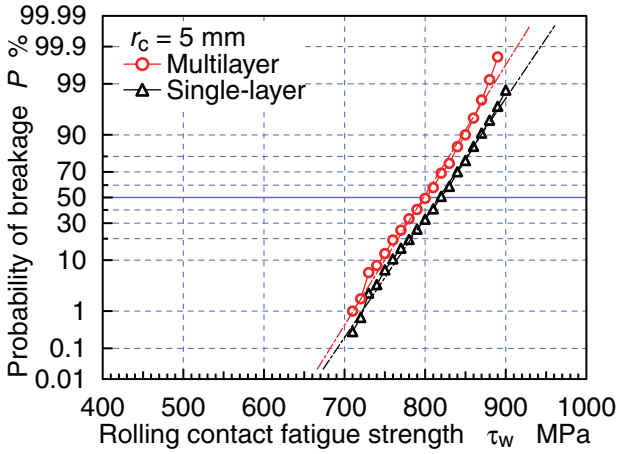

Fig. 11 Normal probability plot (r_c = 5 mm)

Figure 12 is a histogram of the depth of the failure initiation z. Here, z fell between 0.07 mm and 0.36 mm, and almost no change was seen after converting to a multilayered model. As shown in Fig. 8, the shear stress τ_{zx} was particularly high in this region. Figure 13 is a histogram of the $\sqrt{area}$ of the inclusions that were failure initiations. We can see that one consequence of multilayering the model was that the $\sqrt{area}$ was shifted to higher values. Equation (1) predicts that τ_w is lowered as the $\sqrt{area}$ of inclusions increases. Figure 14 shows the sites of failure initiation in the multilayered roller on the xy plane. The origin is the center of the Hertzian contact ellipse and the rolling direction is the positive x direction. The failure initiation sites appear as lines on the coordinate grid because of the change to the multilayered model and also because of the increments in the x direction for the calculations. The reason no failure initiation sites appear in the $x \leq 0$ region is that, due to the traction forces acting on the roller surface, τ_{zx} is high in the $x > 0$ region, as shown in Fig. 8. We can see in this figure that failure is also initiated in the y = 0.1 mm layer. The maximum shear stress in the y = 0.1 mm layer was around 91% of the maximum in the y = 0 mm layer. These figures indicate that the volume that must be evaluated is increased by the changeover to a multilayered model,

and, as a result, this increases the number of inclusions. The numbers of inclusions with high $\sqrt{area}$ increased and some of them were contained in the y = 0.1 mm layer with its lower τ_{zx} levels, but then these inclusions became the failure initiation. Consequently, the shear strength τ_w fell in the multilayered version of the virtual roller.

Comparing the calculated value for the rolling contact fatigue strength τ_w with the experimentally determined τ_w = 790 MPa (Yamanaka et al., 2012), we found the error of the single-layer roller to be 3.4%. The error increased 0.9 points over the error of 2.5% found in the previous report (Narita et al., 2013), but we assume this is due to the tenfold increase in the number of virtual rollers examined. In the multilayered roller, the difference between the calculated 798 MPa and the experimental 790 MPa was only 1.0%. This improvement in the simulation resulted in a reduction of the error by 2.4 points. Multilayering the virtual roller was an effective way to increase the calculation accuracy. The above results justify the use of this improved simulation method to account for the crowning radius of the roller.

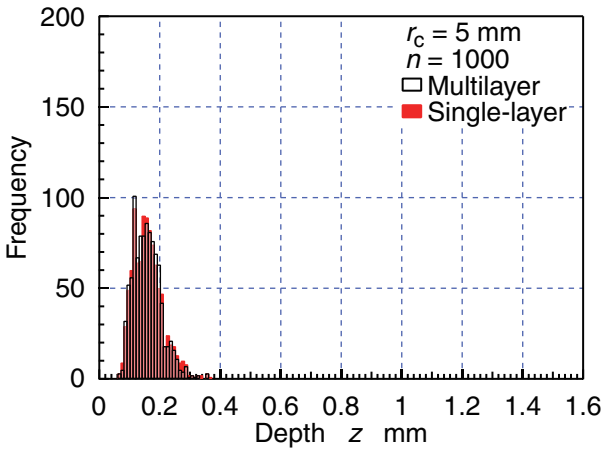

Fig. 12 Depth of failure initiation sites (r_c = 5 mm)

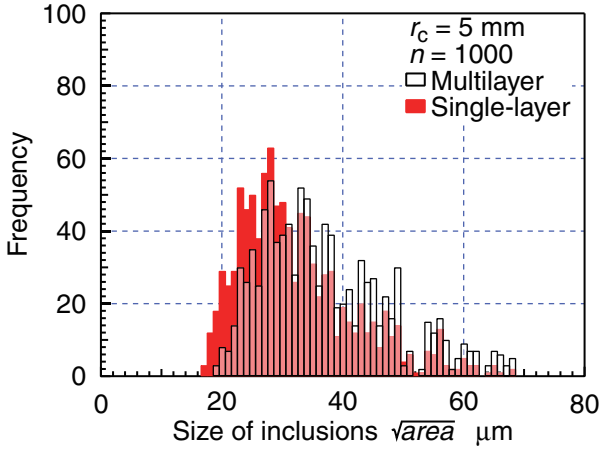

Fig. 13 Size of inclusions of failure initiation sites (r_c = 5 mm)

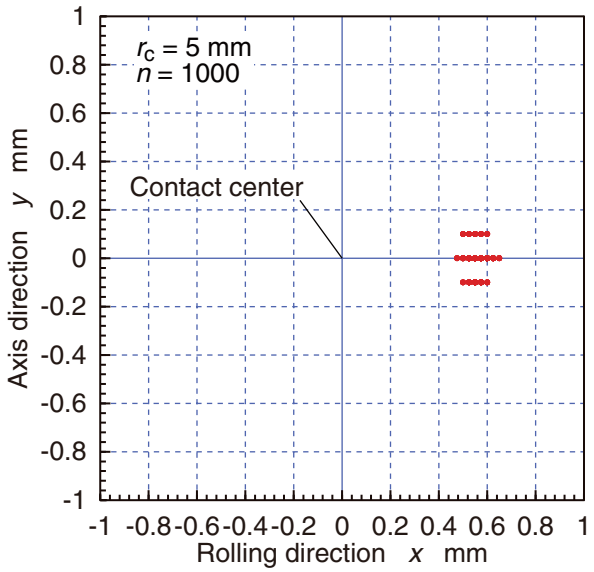

Fig. 14 Distribution of failure initiation sites on contact patch in case of multilayer roller (r_c = 5 mm)

4. Effect of crowning radius

4.1 Rolling contact fatigue strength

Calculations were performed on this improved simulation while varying the crowning radius r_c of the rollers. We observed the influence of the crowning radius on the rolling contact fatigue strength of a traction drive. The simulations analyzed the internal stresses in the driven roller while the crowning radius r_c of the driving roller was varied between 2.5 mm, 10 mm and 100 mm. The rotation radius of the test roller was set to a diameter of 60 mm, as described in the

previous section, and the crowning radius of the driven roller, the object of the evaluation, was flat. The traction coefficient μ was set at the previous value of 0.12, and the hardness distribution was assumed to be that shown in Fig. 7. The calculation range in the y direction was set wide enough to include the most separated layers from y = 0 mm, whose maximum shear stress $\tau_{zx\ max}$ decreased to 50% of $\tau_{zx\ max}$ in the layer at y = 0 mm. The calculations with TED/CPA (Kakoi 1991) indicated 7 layers at r_c = 2.5 mm with -0.3 mm ≤ y ≤ +0.3 mm, 11 layers at r_c = 10 mm with -0.5 ≤ y ≤ +0.5 mm, and 29 layers at r_c = 100 mm with -1.4 mm ≤ y ≤ +1.4 mm.

Table 2 Estimated rolling contact fatigue strength

	Multilayer				Single-layer			
	Crowning radius r_c [mm]				Crowning radius r_c [mm]			
	2.5	5	10	100	2.5	5	10	100
Rolling contact fatigue strength τ_w [MPa]	820	798	785	698	821	817	811	681
Standard deviation σ [MPa]	44.6	39.9	34.1	(61.1)	43.8	41.5	39.7	(92.5)
Contact force F_c [kN]	1.57	1.94	2.57	8.73	1.57	1.99	2.74	9.90

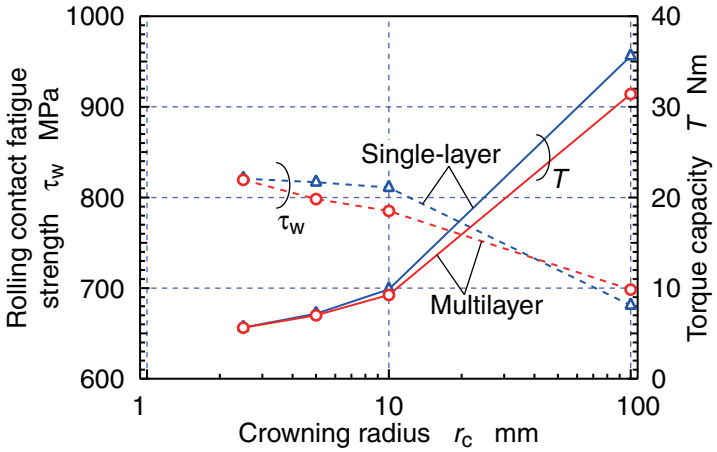

Fig. 15 Relation among estimated rolling contact fatigue strength, torque capacity, and crowning radius

Table 2 shows the rolling contact fatigue strength τ_w calculated for each crowning radius r_c, and Fig. 15 shows how τ_w varied with r_c. These include the results for r_c = 5 mm found in the previous section. Figure 16 provides both histograms and plots of the results on normal probability paper. The findings from the previous single-layer model, where multilayering was not employed, are also plotted here for comparison. Figures 15, 16 and Table 2 indicate that τ_w decreased as r_c was increased. These results echo the findings in the report by Yoshida et al. (1998). Figure 17 shows the failure initiation sites on the xy plane. The reader can see that failure occurred in other layers as well as the y = 0 mm layer, the center of the Hertzian contact ellipse, and that the number of those failure initiation sites outside the y = 0 mm layer increased with the increase of r_c. As shown in Fig. 1, the appropriate volume for examining for high stresses expanded in the y dimension with the increase of r_c. Figure 18 shows the distributions of τ_{zx} for r_c = 2.5 mm and r_c = 100 mm at y = 0 mm. In these graphs, the contact force F_c was adjusted to obtain identical values for the maximum shear stress $\tau_{zx\ max}$. We can also see that the high-stress volume increased in the z direction with the increase in r_c. The spread of the high-stress region in both the y and z directions increased the number of inclusions, and accordingly, increased the number of inclusions with a high $\sqrt{area}$ value. Examining the histograms in Fig. 19 for the $\sqrt{area}$ of the inclusions that were failure initiation sites, we note an increasing frequency of inclusions with a large $\sqrt{area}$ with the increase of r_c. This was the reason for the fall in τ_w with the increase of r_c.

Returning to Fig. 16, we see that the fatigue strength histogram for r_c = 100 mm departs from the normal distribution and that failure occurred in many rollers with low τ_w. The τ_w shown in Table 2 represents values with a 50% probability of failure, calculated by using the normal probability plot up to r_c = 10 mm, but τ_w is the mean of the histogram values at r_c = 100 mm. Figure 20 shows the depths z of the failure initiation sites. An examination of these data shows that the failure was initiated at increasing depths with the increase of r_c. As noted above, the high-stress

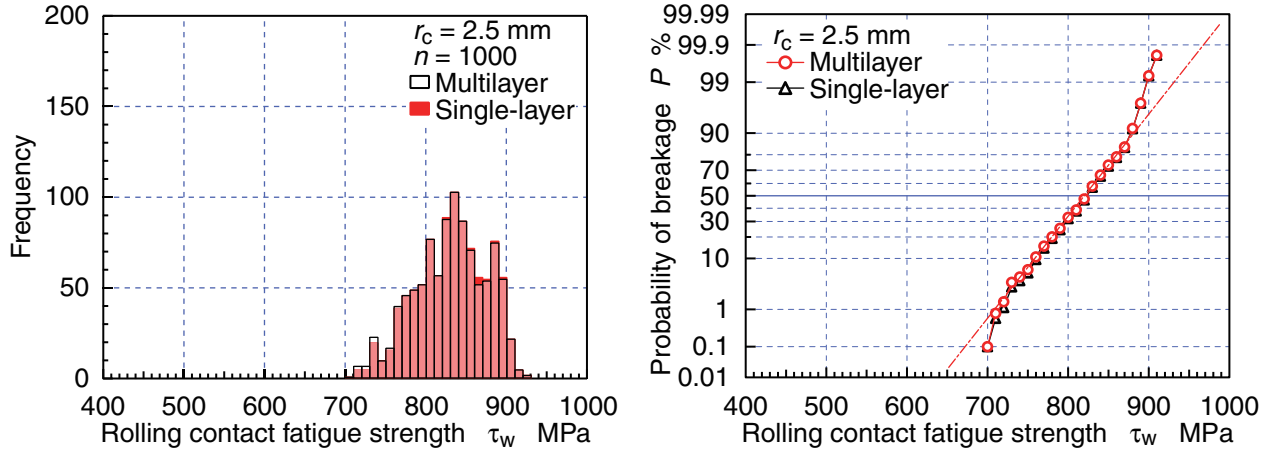

(a) r_c = 2.5 mm

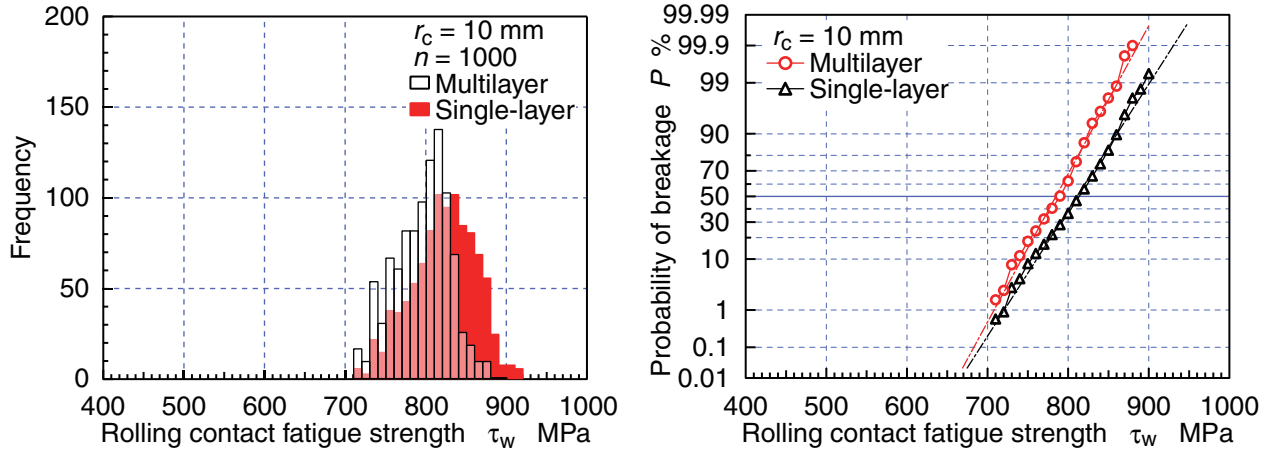

(b) r_c = 10 mm

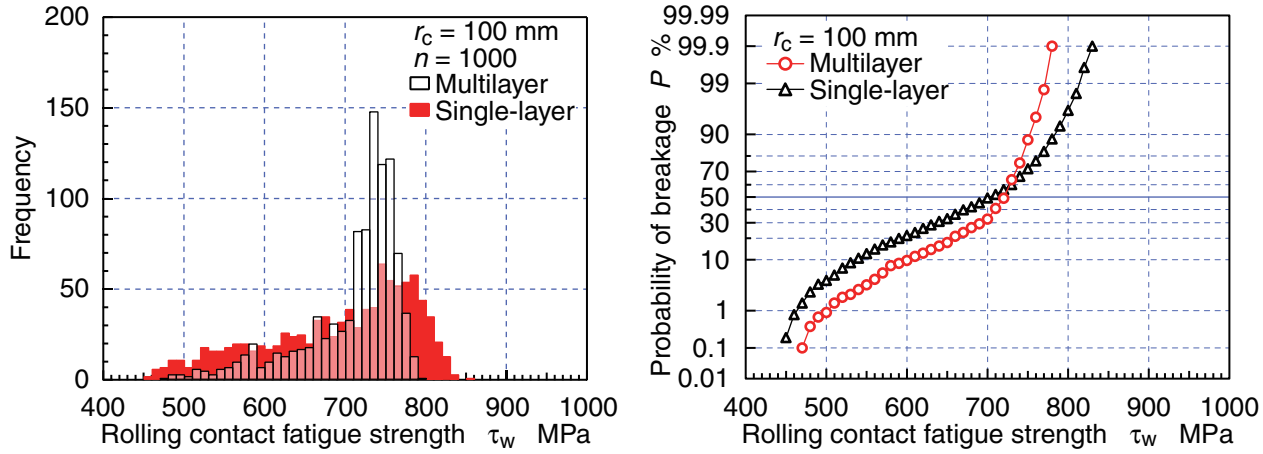

(c) r_c = 100 mm

Fig. 16 Histograms and normal probability plots of estimated rolling contact fatigue strength

region expanded in the z direction with the increase of r_c. In contrast, Vickers hardness H_V decreased with depth z (Fig.7). As indicated in Eq. (1), τ_w decreases when H_V decreases. This is the reason why failure was initiated at deep sites of z, and the low-strength tail of the fatigue strength distribution was enlarged.

4.2 Torque capacity

Finally, we make some observations of the influence of roller crowning radius r_c on the torque capacity T by the

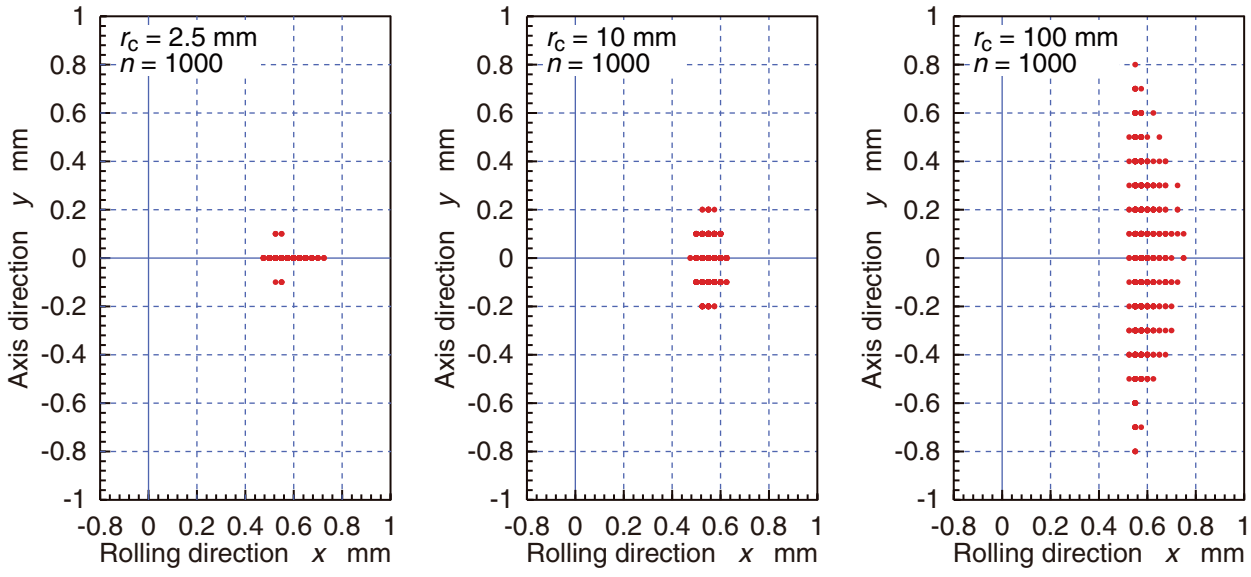

(a) r_c = 2.5 mm (b) r_c = 10 mm (c) r_c = 100 mm

Fig. 17 Distribution of failure initiation sites on contact patch in case of multilayer roller

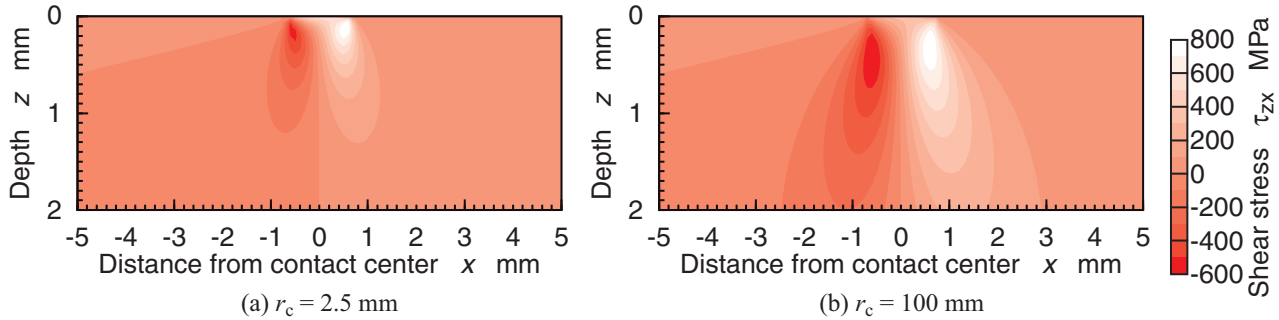

(a) r_c = 2.5 mm (b) r_c = 100 mm

Fig. 18 Shear stress τ_{zx} of driven roller

simulation. The torque capacity T at each r_c was obtained by multiplying the mean value of the calculated contact force F_c at the failure initiation by the traction coefficient μ = 0.12 and by the roller rotation radius r = 30 mm; the corresponding mean values F_c are also presented in Table 2. The calculated values for T are presented in Fig. 15. It is clear that T increases with r_c. These results suggest that increasing the crowning radius can increase the torque capacity of a traction drive. And Fig.15 enables us to find the minimum crowning radius preventing the failure for the required torque capacity.

5. Conclusion

The simulation of the rolling contact fatigue strength in traction drives proposed in a previous report was improved and the influence of the crowning radius on rolling contact fatigue strength and on torque capacity of traction drive was evaluated. The following results were obtained:

(1) The simplified method of converting a two-dimensional virtual roller model into a three-dimensional one by using multiple layers allowed us to conduct simulations that accounted for the crowning radius.

(2) A simulation was conducted on the rolling contact fatigue strength in a roller with a crowning radius of 5 mm, the value used in an actual experiment, and an error of 1.0% from the experimental values was achieved in the multilayered roller model. In comparison, this was 2.4 points lower than the error of the previous single-layer model.

(3) The simulation was repeated while varying the crowning radius. The rolling contact fatigue strength decreased with the increase of the crowning radius. This was attributed to the increase in volume of the high-stress region, resulting in an increase in the number of inclusions, and to the enlarged high-stress region extending into the

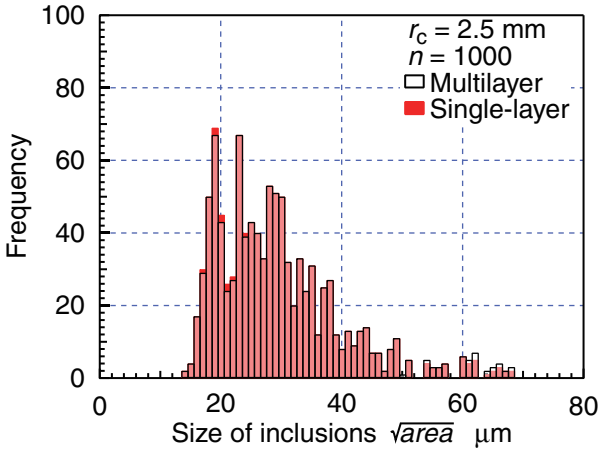

(a) r_c = 2.5 mm

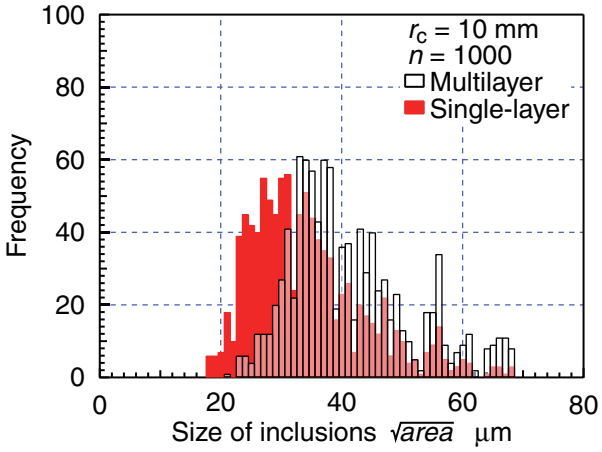

(b) r_c = 10 mm

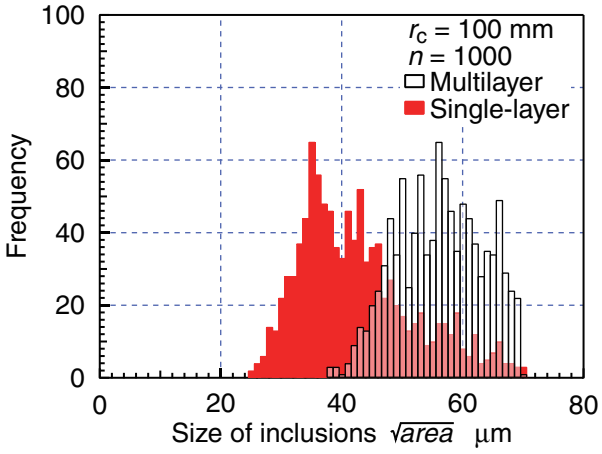

(c) r_c = 100 mm

Fig. 19 Histograms of inclusion sizes of failure initiation sites

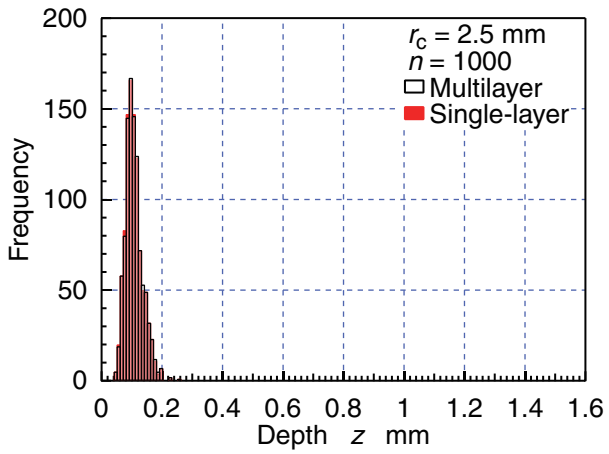

(a) r_c = 2.5 mm

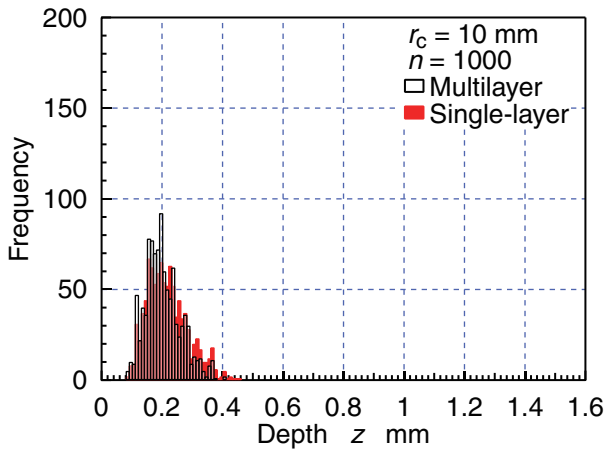

(b) r_c = 10 mm

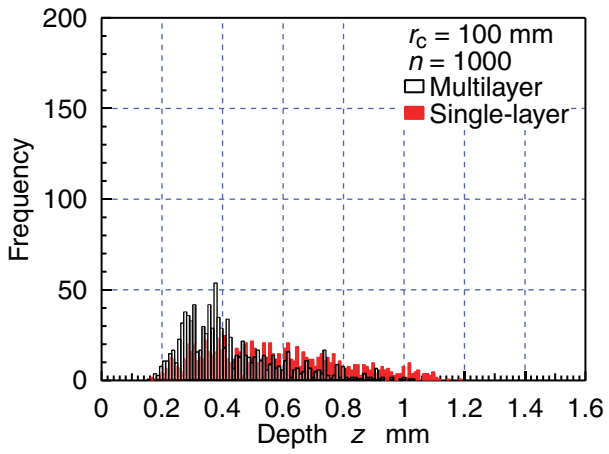

(c) r_c = 100 mm

Fig. 20 Histograms of depth of failure initiation sites

depths with lower hardness.

(4) The torque capacity was calculated by using the mean contact force at the failure initiation, obtained by the above simulation, and the torque capacity was found to be increased by increasing the crowning radius.

Acknowledgement

This study was made possible by a Grant-in-Aid for Scientific Research (Grant-in-Aid for Young Scientists (B),

No.25820028, 2013) by the Japan Society for the Promotion of Science. We offer our deep thanks for this assistance.

References

Coy, J. J., Rohn, D. A., and Loewenthal, S. H., Constrained fatigue life optimization of a Nasvytis multiroller traction drive, Transaction of the American Society of Mechanical Engineers, Journal of Mechanical Design, Vol. 103 (1981), pp. 423-428.

Deng, G., Yamanaka, M., Yamamoto, R., Ono, N., Kato, M., and Inoue, K., Contact fatigue and strength evaluation of traction drive rollers, Transactions of the Japan Society of Mechanical Engineers, Series C, Vol. 65, No. 635 (1999), pp. 2880-2885 (in Japanese).

Fujii, M., Bayasgalan, S., Yoshida, A., Hamada,K., Minegishi, K., and Tamenaga, J., Influence of crowning on rolling contact fatigue strength and failure mode of steel roller, Transactions of the Japan Society of Mechanical Engineers, Series C, Vol.73, No.728 (2007), pp.1222-1229 (in Japanese).

Kakoi, K., Numerical Analysis of 3-dimensional contact problems with friction by special boundary element method, Transactions of the Japan Society of Mechanical Engineers, Series A, Vol. 57, No. 544 (1991), pp. 3010-3015 (in Japanese).

Machida, H., Hata, H., Nakano, M., and Tanaka, H., Half-toroidal traction drive continuously variable transmission for automobile propulsion systems (traction drive materials, transmission design and efficiency), Transactions of the Japan Society of Mechanical Engineers, Series C, Vol. 59, No. 560 (1993), pp. 1154-1160 (in Japanese).

Machida, H., Itoh, H., Imanishi, T., and Tanaka, H., Design principle of high power traction drive CVT, SAE paper, 950675, (1995).

Masuyama, T., Asano, J., and Inoue, K., Fatigue strength simulation of carburized gears based on Weibull distribution of inclusions, Proc. JSME, No. 02-12 (2002a), pp. 33-36 (in Japanese).

Masuyama, T., and Katsumi INOUE, Computation of fatigue strength of carburized gears based on simulated distribution of defects, Proceedings of International Conference on Gears, VDI-Berichte, Nr. 1665 (2002b), pp. 421 - 434.

Matsuo, K., Saeki, S., Ooue, Y., and Yoshida, A., Effect of traction fluid on rolling contact fatigue life of thermally refined steel, Tribology Series, Vol.18 (1991), pp. 445–450.

Murakami, H., Estimation of rolling contact fatigue life due to determination of non-metallic inclusions, NTN Technical Review, No. 68 (2000), pp. 58-62 (in Japanese).

Murakami, Y., Metal fatigue: effects of small defects and nonmetallic inclusions, Elsevier, (2002).

Murakami, Y., Kodama, S., and Konuma, S., Quantitative evaluation of effects of nonmetallic inclusions on fatigue strength of high strength steel, Transactions of the Japan Society of Mechanical Engineers, Series A, Vol. 54, No. 500 (1988), pp. 688-696 (in Japanese).

Nakajima, A., and Mawatari, T., Rolling contact fatigue life of bearing steel rollers lubricated with low viscosity traction oil, Tribology and Interface Engineering Series, Vol. 48 (2005), pp. 351-362.

Narita, Y., Yamanaka, M., Kazama, T., Osafune, Y., and Masuyama, T., Simulation of rolling contact fatigue strength for traction drive elements, Journal of Advanced Mechanical Design, System and Manufacturing, Vol.7, No.3 (2013), pp. 432-447.

Rohn, D. A., Loewenthal, S. H., and Coy, J. J., Simplified fatigue life analysis for traction drive contacts, Transaction of the American Society of Mechanical Engineers, Journal of Mechanical Design, Vol. 103 (1981), pp. 430-439.

Yamanaka, M., Yamamura, J., Narita, Y., and Inoue, K., Evaluation of rolling contact fatigue strength for traction-drive elements by using artificial defect, Journal of Japan Society for Design Engineering, Vol. 47, No. 5 (2012), pp. 252-258 (in Japanese).

Yoshida, A., Ohue, Y., Matsuo, K., Saeki, S., and Hayakawa, T., Effect of crowning radius on rolling contact fatigue strength of case-hardened steel roller, Transactions of the Japan Society of Mechanical Engineers, Series C, Vol.64, No.626 (1998), pp.3982-3988 (in Japanese).

Yoshida, A., Ohue, Y., Hara, T., Fujita, K., Miyanisi, K., and Torii, O., Effect of hardened depth and relative radius of curvature on surface durability of a carbonitrided SCr420 steel roller, Transactions of the Japan Society of Mechanical Engineers, Series C, Vol.55, No.518 (1989), pp.2591-2598 (in Japanese).